IEEE/CSC & ESAS European Superconductivity News Forum (ESNF), No. 6, October 2008
(ASC Preprint 2EPE02 conforming to IEEE Policy on Electronic Dissemination, Section 8.1.9)

The published version of this manuscript appeared in *IEEE Transactions on Applied Superconductivity* **19**, No. 3, Part 1, 697 - 701 (2009)

Miniature Thin-Film SQUID Susceptometer for Magnetic Microcalorimetry and Thermometry

S. T. P. Boyd, Vincent Kotsubo, Robin Cantor, Alexander Theodorou, and J. Ad Hall

***Abstract*— We have developed a miniature thin-film SQUID susceptometer for research in magnetic microcalorimetry and miniature magnetic thermometry. We have previously reported measurements at 4K characterizing performance of the first generation of this device using modulation-based flux-locked feedback electronics and at ~50mK using a spherical superconducting test sample. Here we describe design, fabrication, and new measurements of the second generation of the device using two-stage SQUID amplification to characterize the improved noise, bandwidth, persistence switch and field coil performance. The device now meets or exceeds all requirements for magnetic microcalorimetry sensor testing, achieving noise of ~0.75μΦ_0/√Hz and bandwidth ~1.2MHz near 50mK, and trapping and stably holding magnetizing field of at least 5.9mT.**

***Index Terms*— Detectors, SQUID magnetometers, Superconducting switches**

I. INTRODUCTION

DETERMINING the temperature of a paramagnet by measuring its magnetization is a powerful technique in low-temperature physics. It has been used for magnetic thermometry at least since the first data was taken below 1 K [1], and remains an active area of research in modern SQUID-based measurements, yielding in recent years thermometers capable of 0.1 nK/√Hz resolution near 1 Hz at 2.2 K [2], [3], among other efforts [4]-[6].

Recently it was shown that this technique is also an important new approach for low-temperature microcalorimetry [7]. In 2007 energy resolution of 2.7 eV for 6 keV photons was demonstrated for a device using a metallic paramagnetic sensor with SQUID readout [8]. This "metallic magnetic microcalorimeter" (MMC) performance is already comparable with the best performance from the more well-established superconducting transition-edge sensor (TES) approach.

Low-temperature microcalorimetry is an important new area of research because it brings new detection physics to the important problems of radiation and particle detection. Magnetic microcalorimetry is again an important new area within low-temperature microcalorimetry because it brings alternative new detection physics.

The new detection physics of MMC differs from TES at the most fundamental level. MMC is a measurement of an equilibrium thermodynamic property, magnetization, which can be determined from first principles, and the power dissipation associated with the measurement can be made almost arbitrarily small. By contrast TES is a measurement of a transport property, electrical resistance, that is understood largely phenomenologically and intrinsically requires power dissipation.

The new magnetic approach to particle detection offers new capabilities and constraints relative to the TES approach. We are presently investigating the suitability of the dilute Pd:Fe alloy paramagnet [9]-[11] for microcalorimetry. As part of this effort we have developed a new miniature monolithic thin-film SQUID susceptometer with integrated field coils and persistence switch suitable for measurements on microsamples ~50μm diameter and smaller at temperatures down to (at least) 50 mK. This device is in part a hybrid of the approaches of Ketchen [12], [13] and the Jena/Heidelberg collaboration [14], [15]. We have previously reported measurements characterizing the first generation of this device with modulation electronics [11], [16]. We describe here the new susceptometer's design and fabrication, and its performance with two-stage SQUID amplification and test microsamples.

II. DESIGN REQUIREMENTS

Design requirements for microcalorimetry were developed using two numerical models: 1) a simplified model of the paramagnetic alloy microsample calculating magnetization and entropy for free spins [17], including both nuclear and electronic spin systems, plus the linearly temperature dependent electronic heat capacity; and 2) a 2D axisymmetric finite element model of the magnetic geometry including the microsample and the superconducting pickup loop and field coil. These models were constructed using MATLAB [18] and FEMM [19] and will be described fully elsewhere.

In combination, these models show that, given: 1) the target paramagnetic alloy, Pd:Fe 200 at. ppm; 2) the geometry of the microsample, pickup loop, and field coils (described below); and 3) the temperature range accessible in our adiabatic demagnetization refrigerator cryostat, the maximum flux responsivity (the flux change in the SQUID for a given energy input to the microsample) is obtained at the lowest temperature available, 50 mK, and in a magnetic field strength $\mu_0 H$ = 3.0 mT. This sets the requirements for operating

Manuscript received 19 August 2008. This work was supported by the U.S. Defense Threat Reduction Agency.

S. Boyd, V. Kotsubo, and A. Theodorou, are with the Department of Physics and Astronomy, University of New Mexico, MSC07-4220, Albuquerque, NM 87131-0001 USA (corresponding author: S. Boyd, phone: 505-277-4439; fax: 505-277-1520; e-mail: stpboyd@unm.edu; V. Kotsubo email: vkotsubo@earthlink.net; A. Theodorou email: alext@unm.edu).

R. Cantor and J. Hall are with STAR Cryoelectronics, Santa Fe, NM, 87508 USA. (R. Cantor email: rcantor@starcryo.com; J. Hall email: ahall@starcryo.com).

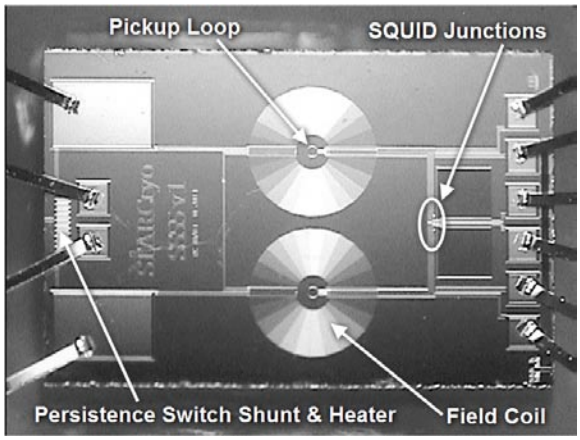

Fig. 1. Photograph of the 2 mm × 3 mm susceptometer. The large bonding pads on the left are for the field coil circuit, the small pads are for the persistence switch heater. Pads on the right are for SQUID bias and feedback.

temperature and magnetizing field.

The fast magnetization dynamics associated with particle energy deposition [7] set a requirement for high-bandwidth two-stage SQUID amplification with direct readout.

Given that the energy resolution of the microcalorimeter will be limited by thermal fluctuation noise to > 1 eV, the flux noise ~2.5μ$\Phi_0/\sqrt{\text{Hz}}$ previously seen [16] is already more than adequate. However, the requirement for maximum bandwidth drives a requirement for maximum SQUID dV/dφ, which will also act to lower the flux noise.

III. Design

The photograph in Fig. 1 shows the layout of the new susceptometer. Basic design features and functions have been described previously [11], [16]. We will include some of this background information here to make this report more self-contained, while concentrating on new or changed features.

The two counter-wound pickup loops form a first-order gradiometer that is part of the SQUID loop. For balanced gradiometric design the layout has mirror symmetry about the horizontal midline of the chip. Integral field coils eliminate microphonics and concentrate field at the microsample and away from the SQUID junctions. The field coils are connected in series, are centered on the pickup loops, and apply equal and parallel magnetizing fields. The superconducting field coil circuit is persistent, using the persistence shunt and heater on the left side of the chip.

The pickup loop spacing has been increased to 800 μm to accommodate larger field coils. Each loop is a single turn of Nb 650 nm thick and 3.5 μm wide, with inner diameter increased to 55 μm. The calculated self-inductance of each pickup loop is 120 pH, which increases by ~2% at 50 mK with a 50 μm-dia × 12.5 μm tall Pd:Fe microsample mounted.

The SQUID loop is formed by the pickup loops and the interconnecting traces to the SQUID junctions. The interconnecting traces are fabricated on top of a Nb ground plane to reduce pickup and parasitic inductance, which is estimated as ~30 pH. Thus the total estimated SQUID loop self-inductance is ~270 pH.

The flux concentrating washer of the previous field coil design [11], [16] was eliminated to improve homogeneity of the magnetizing field over the microsample volume and to avoid trapping flux. To compensate, the number of turns was increased to 38. The new spirals have 200 μm inner diameter and 728 μm outer diameter, with Nb traces 1.1 μm thick, 5 μm wide, with 2 μm spacing. The narrow trace width w=5 μm should allow the field coil spirals to completely expel flux vortices for cooling fields up to ~Φ_0/w^2=~80 μT [20].

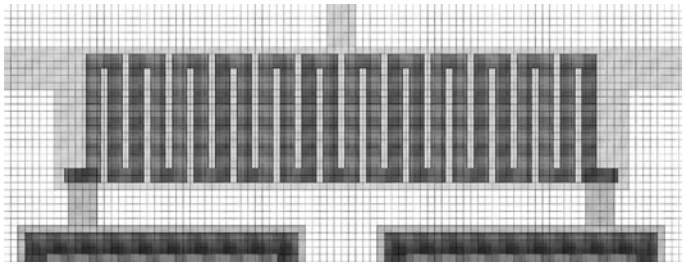

Fig. 2. Persistence switch layout, rotated 90º from Fig. 1. The grid is 5 μm squares. The dark gray meander is the heater (~265 nm Au:Pd), with downward connections to the heater pads. The light gray film under the heater is the Nb shunt (anodized Nb: ~230 nm Nb with 120 nm Nb_2O_5 on top), with sideways connections to the field coil pads. The upward connection is unused. The whole structure is covered with about 400 nm of PECVD SiO_2.

Removal of the flux-concentrating washer increases the field leakage from the field coils, so the 120 mT/A central field calculated for an isolated field coil is reduced slightly to 118 mT/A by the field from the other coil. Similarly the calculated self-inductance of each field coil is reduced from 627 nH to 612 nH. Leakage field from the two spirals adds to 3.8 mT/A at the SQUID junctions. The required current to reach the operating field strength of 3 mT is 25.4 mA, and at that current the leakage field at the junctions is ~100 μT.

Details of the new persistence switch are shown in Fig. 2. To increase current-carrying capacity, the Nb shunt vertical width was increased. Thermal isolation was improved to increase current-switching capacity: the heater and shunt were narrowed horizontally to increase the distance to the field coil pads, and moved to the edge of the die to be as far as possible from the field coil spirals and interconnects. The trace connecting the two field coils was also moved closer to the spirals to increase its distance from the heater.

IV. Fabrication

The susceptometers are fabricated using a six-layer process based on a Nb/Al-AlO_x/Nb trilayer process for 100- and 150-mm diameter oxidized Si wafers described previously [21]. As with the previous generation of the device [11], [16], the process differs slightly from [21] in that the resistors are made using Au:Pd alloy (48%/52%) rather than pure Pd, and patterned using liftoff. For the current generation the thickness of the second Nb wiring layer has been increased to 1.1 μm and it has been patterned with a Reactive Ion Etch (RIE) process.

V. Measurements

Measurements were performed in an adiabatic demagnetization refrigerator cryostat. The two-stage SQUID amplification and readout used STAR Cryoelectronics series SQUID array AR232, programmable feedback loop PFL-102, and PC interface readout electronics PCI-1000 [22].

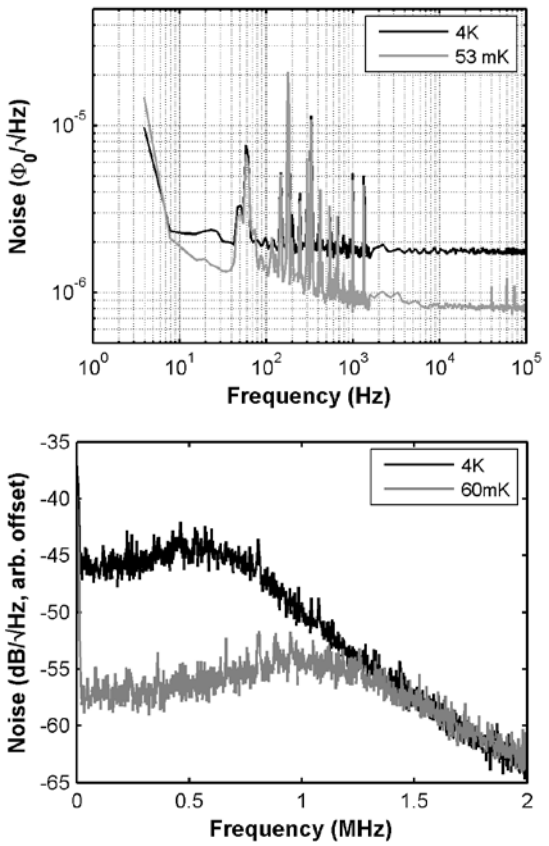

Fig. 3. (Upper) Typical 100 kHz noise spectra. (Lower) Typical 2 MHz noise spectra. Susceptometer was "bare" in upper plot, "loaded" with test Pd microsample in lower plot.

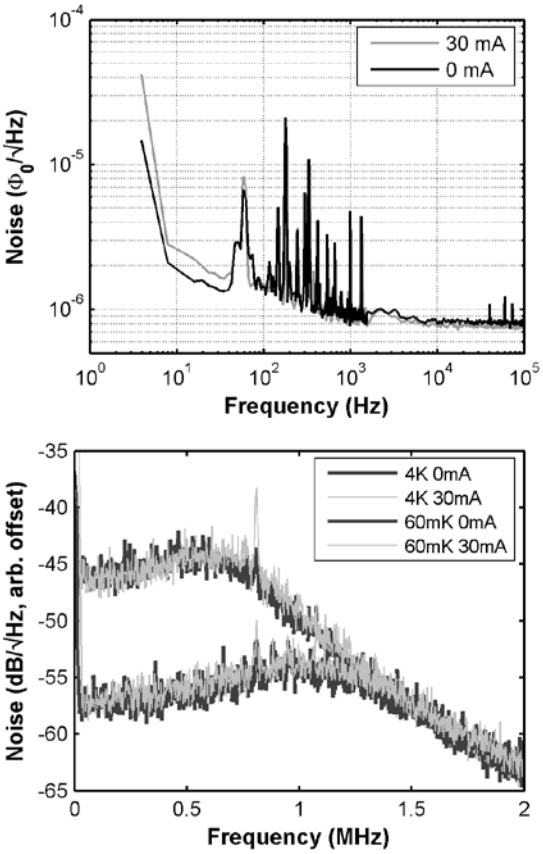

Fig. 4. Impact of trapped field coil current on noise and bandwidth. (Upper) 100 kHz noise spectra near 60mK with 0 and 30 mA trapped. (Lower) 2 MHz noise spectra at 4K (upper traces) and 60 mK (lower traces) for 0 and 30 mA trapped. The susceptometer was "bare" in upper plot, "loaded" in lower plot.

A. Noise and Bandwidth

Fig. 3 shows typical 100 kHz noise spectra at 4 K and 53 mK, and 2 MHz noise spectra at 4 K and 60 mK. Table I summarizes typical noise and bandwidth values. Compared to tests on the previous device with modulation electronics [11], [16], tests on the new device with two-stage SQUID amplification realize three improvements: 1) a substantial reduction in the noise near 50 mK (0.75 $\mu\Phi_0/\sqrt{Hz}$ versus 2.5 $\mu\Phi_0/\sqrt{Hz}$); 2) a large increase in the bandwidth (~1.2 MHz versus ~50 kHz); and 3) a large improvement in the reduction of noise upon cooling from 4 K to 50 mK.

Note that the noise level is affected by the presence or absence of the microsample through the magnetic Johnson noise, as described below, but the bandwidth is not. Note also that ~0.6 $\mu\Phi_0/\sqrt{Hz}$ and ~1.2 MHz are the noise floor and bandwidth ceiling set by the SQUID array/readout electronics.

B. Impact of Field Coil Current

Fig. 4 shows that a trapped current of 30 mA, slightly greater than the design current of 25 mA, has no discernable impact on the bandwidth of the new susceptometer at 4 K or 60 mK. SQUID tuning parameters were not changed by the presence of the field. The trapped current does appear to cause a slight increase in noise at frequencies below ~100 Hz, rising to a noise increment of about ~1 $\mu\Phi_0/\sqrt{Hz}$ at 10 Hz. The 100 kHz spectrum at 4 K shows the same slight increase.

TABLE I TYPICAL NOISE AND BANDWIDTH PERFORMANCE

Temperature	Noise ($\mu\Phi_0/\sqrt{Hz}$)	Bandwidth (MHz)
4K	1.8-2.0	0.65-1.1
Near 50mK	0.65-0.85	1.1-1.4

C. Magnetic Johnson Noise and Microsample Conductivity

"Magnetic Johnson Noise" (MJN) is the term which has been adopted to describe the flux noise induced in the SQUID loop by thermal excitation of eddy currents in the metallic microsample. As a consequence of the Fluctuation-Dissipation Theorem [23], the noise voltage induced in the SQUID loop at a given frequency by the MJN can be easily determined if we can calculate the power dissipation in the microsample that would result from an AC current in the SQUID loop at the same frequency [24]. Given values for the electrical conductivity and relative magnetic permeability of the microsample, this dissipation can be calculated by our numerical magnetic geometry model in the harmonic approximation. It is then straightforward to calculate the flux noise induced in the SQUID loop by the MJN. By comparing the calculated MJN to measured noise spectra we can then estimate the electrical conductivity of the microsample.

Fig. 5 shows measured noise spectra at 4K for a susceptometer with and without a microsample mounted. These spectra indicate an MJN contribution of $\sqrt{(5.52-1.82)}$ = 5.2 $\mu\Phi_0/\sqrt{Hz}$ at 4K. The magnetic geometry model calculation for this sample geometry predicts an MJN

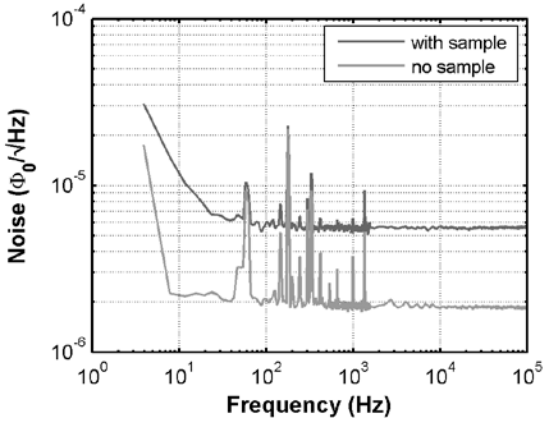

Fig. 5. Magnetic Johnson noise caused by the metallic microsample. This figure shows two noise spectra at 4K for a magnetometer with and without a microsample mounted.

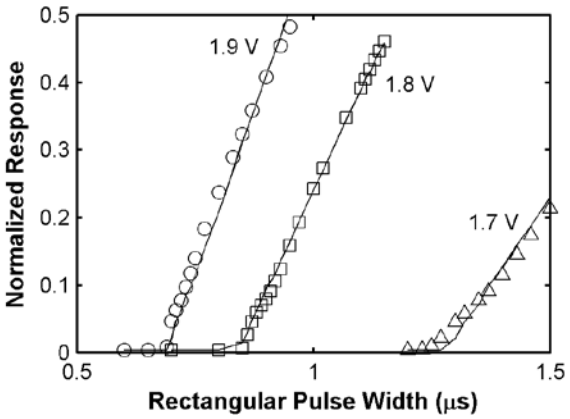

Fig. 6. "Normalized Response" of the persistence switch versus the width of the rectangular heater pulse, for three pulse heights. Pulsing rate was 20 Hz for this data. The points are the measured data, the lines are the fits obtained with the simple lumped-element model.

spectrum which is flat up to a resistivity-dependent roll-off frequency. The low-frequency MJN level matches the level shown in Fig. 5 if we assume a 4 K electrical resistivity of 0.155 μΩ·cm. (This calculation also yields an MJN roll-off frequency ~5 MHz.)

Measurement of the 99.95% pure Pd foil stock from which this test microsample was fabricated found a room-temperature resistivity of 9.5 μΩ·cm and RRR=43, and thus an electrical resistivity of 0.22 μΩ·cm at 4K.

The 30% level of agreement between the calculation for the microsample and the measurement of the foil stock is reasonable given the small, but nonzero, imprecision in the modeled magnetic geometry and in the physical placement of the microsample within the pickup loop. However, the fact that the resistivity values of the microsample and the starting foil are comparable provides some confidence that the microsample fabrication process (ion milling) is not causing gross damage to the crystal structure of the microsample.

D.Persistence Switch Testing and Performance

The thin-film heated persistence switch was able to trap and hold currents of 50 mA and more, well above the 25 mA design current. As with the previous version of the switch [11], [16], actuation in vacuum was accomplished by short rectangular voltage pulses, typically 1 μs wide by ~1.8 V tall. For current trapping we would typically pulse the heater at ~20 Hz, yielding an effective L/R time constant of a few seconds. Alternatively, a steady 1.4 V across the heater sufficed to drive the SQUID normal in a few seconds for flux expulsion.

Stability of the trapped current was confirmed in two ways. The first approach used the suppression of the superconducting transition temperature T_c of a ~25 μm diameter Al microsphere mounted in one pickup loop. Although the magnetization signal on cooling the Al microsphere through T_c in field was complicated, the signal on warming through T_c was reproducible, and showed that the trapped current was stable for at least 3.5 hours, the longest test interval.

The second approach to stability testing was by monitoring the slewing of the V-φ curve of the SQUID. There was a small mutual inductance between the field coil circuit and the SQUID loop due to imbalance, so any slewing of the V-φ curve along the φ-axis when the persistence switch was pulsed indicated a mismatch between the externally applied field coil current and the trapped current. This test could be performed quickly at any temperature, and confirmed stability of the trapped current for at least ~12 hours, the longest test interval.

We used an AC measurement technique to study the properties of the pulsed persistence switch in the presence of the parallel inductive short formed by the field coil circuit. In this set-up a lock-in measured the SQUID response to a 1 Hz signal applied to the field coil leads while the height, width, and frequency of the heater pulses were varied. The "normalized response" (RMS SQUID response divided by RMS excitation voltage) is shown in Fig. 6, demonstrating the sharp turn-on of the persistence switch as a function of pulse width for various pulse heights. From this and other quantitative data obtained with the AC technique we were able to fit component values for a simple lumped-element coupled electro-thermal model which describes the persistence switch function quite well, as shown by the curves in Fig. 6. A full description of this new method and results will be presented in a future report.

VI. Conclusion

The measurements reported here demonstrate that the new generation of the micro-susceptometer meets or exceeds the temperature, field, noise, and bandwidth requirements for magnetic microcalorimetry testing with our target sensor material Pd:Fe. Initial measurements of the temperature and field dependence of the magnetization of Pd:Fe microsamples are now underway.

Acknowledgment

S. Boyd thanks Christian Enss and Andreas Fleischmann of the University of Heidelberg for numerous helpful discussions. S. Boyd and R. Cantor are grateful to Kent Irwin and Joel Ullom of NIST for agreeing to share V. Kotsubo's time between our projects, and for help debugging our ADR.

REFERENCES

[1] W. F. Giauque, and D. P. MacDougall, "Attainment of temperatures below 1º absolute by demagnetization of $Gd_2(SO_4)_3$ $8H_2O$," *Phys. Rev.* vol. 43, p. 768-768, May 1933.

[2] D. A. Sergatskov, P. K. Day, A. V. Babkin, R. C. Nelson, T. D. McCarson, S. T. P. Boyd, R. V. Duncan, "New paramagnetic susceptibility thermometers for fundamental physics measurements," *AIP Conf. Proc.*, vol. 684, pp. 1009-13, Sept. 2003.

[3] B. J. Klemme, M.J. Adriaans, P. K. Day, D. A. Sergatskov, T. L. Aselage, R. V. Duncan, "PdMn and PdFe: new materials for temperature measurement near 2K," *J. Low Temp. Phys.* vol. 116, pp. 133-146, Feb. 1999.

[4] J. G. Tuttle, M. J. DiPirro, E. R. Canavan, P. J. Shirron, E. Kunes, and T. P. Hait, "A miniature palladium-iron thermometer for temperatures down to 0.05 Kelvin," *AIP Conf. Proc.*, vol. 613B, pp. 1613-1619, 2002.

[5] J. G. Tuttle, T. R. Stevenson, E. R. Canavan, M. J. DiPirro, D. E. Franz, and P. J. Shirron, "A deposited magnetic thermometer for temperatures below 0.1 Kelvin," *AIP Conf. Proc.*, vol. 710, pt.1, pp. 396-403, 2004.

[6] M. Jutzler; B. Schroder; K. Gloos, F. Pobell, "Palladium-iron - a giant-moment magnetic thermometer for the millikelvin temperature-range," *Zeitschrift Fur Physik B-Condensed Matter*, v.64, no.1, p.115-118, 1986.

[7] A. Fleischmann, C. Enss, and G. M. Seidel, "Metallic Magnetic Calorimeters," in *Cryogenic Particle Detection*, C. Enss, Ed. Berlin: Springer-Verlag, 2005, pp. 151–216.

[8] L. Fleischmann, presentation at the 12th International Workshop on Low-Temperature Detectors (LTD12), Paris, July 22-27, 2007.

[9] G. J. Nieuwenhuys, "Magnetic behavior of cobalt, iron, and manganese dissolved in palladium," *Advances in Physics*, vol. 24, pp. 515-591, July 1975.

[10] R. P. Peters, Ch. Buchal, M. Kubota, R. M. Mueller, and F. Pobell, "Palladium-Iron: A giant-moment spin-glass at ultralow temperatures," *Phys. Rev. Lett.*, vol. 53, pp 1108-1111, Sept. 1984;

[11] R. Cantor, J. A. Hall, P. Blumenfeld, S. T. P. Boyd, "Miniature thin-film superconducting quantum interference device susceptometer," *IEEE Trans. Appl. Superconductivity*, vol. 17, no. 2, pt. 1, pp. 738-741, Jun. 2007.

[12] M. B. Ketchen, T. Kopley, and H. Ling, "Miniature SQUID susceptometer," *Appl. Phys. Lett.* Vol. 44, pp. 1008-1010, May 1984.

[13] M. B. Ketchen, D. D. Awschalom, W. J. Gallagher, A. W. Kleinsasser, R. L. Sandstrom, J. R. Rozen, and B. Bumble, "Design, fabrication, and performance of integrated miniature SQUID susceptometers," *IEEE Trans. Magn.* vol. 25, pp. 1212-1215, March 1989.

[14] V. Zakosarenko, R. Stolz, L. Fritzsch, H.G. Meyer, A. Fleischmann, C. Enss, "SQUID gradiometer for ultra-low temperature magnetic microcalorimeter", *Supercond. Sci. Technol.* 16, pp. 1404-1407, Dec. 2003.

[15] R. Stolz, V. Zakosarenko, S. Anders, L. Fritzsch, H.-G. Meyer, A. Fleischmann, and C. Enss, "SQUID-Gradiometers for Arrays of integrated Low Temperature Magnetic Micro-Calorimeters" *IEEE Trans. Appl. Superconductivity* Vol. 15, pp. 773-776, June 2005.

[16] S. T. P. Boyd, R. Cantor, V. Kotsubo, P. Blumenfeld, J. A. Hall, "Characterization of a miniature thin-film SQUID susceptometer for metallic magnetic microcalorimetry" *J. Low Temp. Phys.* v.151, no.1-2, pp. 369-374, Apr. 2008.

[17] R. P. Hudson, *Principles and Application of Magnetic Cooling*, Amsterdam: North-Holland, 1972, pp. 3-13.

[18] The MathWorks, Inc, 3 Apple Hill Drive, Natick, MA 01760-2098. http://www.mathworks.com/.

[19] http://femm.foster-miller.net/.

[20] G. Stan, S. B. Field, and J. M. Martinis, "Critical field for complete vortex expulsion from narrow superconducting strips," *Phys. Rev. Lett.*, vol. 92, 097003, March 2004.

[21] R. Cantor and J. Hall, "Six-layer process for the fabrication of Nb/Al-AlOx/Nb Josephson junction devices," *IEEE Trans. Appl. Superconductivity* vol. 15, pp. 82-85, June 2005.

[22] STAR Cryoelectronics, 25-A Bisbee Court, Santa Fe, NM 87508-1412. http://www.starcryo.com.

[23] H. B. Callen and T. A. Welton, "Irreversibility and generalized noise," *Physical Review*, vol. 83, no. 1, pp. 34-40, July 1951.

[24] J. T. Harding and J. E. Zimmerman, "Quantum interference magnetometry and thermal noise from a conducting environment" *Physics Letters* A, vol. 27, pp. 670-671, October 1968.